Christopher Earls Brennen
Hayman Professor of Mechanical Engineering
Emeritus,
California Institute of Technology,
Pasadena, CA 91125

A Review of the Dynamics of Cavitating Pumps

This paper presents a review of some of the recent developments in our understanding of the dynamics and instabilities caused by cavitation in pumps. Focus is placed on presently available data for the transfer functions for cavitating pumps and inducers, particularly on the compliance and mass flow gain factor, which are so critical for pump and system stability. The resonant frequency for cavitating pumps is introduced and contexted. Finally, emphasis is placed on the paucity of our understanding of pump dynamics when the device or system is subjected to global oscillation. [DOI: 10.1115/1.4023663]

1 Introduction

Since the first experimental measurements many years ago of the complete dynamic transfer function for a cavitating pump [1,2], there has been a general recognition of the importance of various components of these transfer functions (particularly the cavitation compliance and mass flow gain factor) in determining the dynamic characteristics and instabilities of systems incorporating such pumps (see, for example, Refs. [3–7]). The present paper attempts to summarize some of the recent understandings and to evaluate the current state of knowledge of transfer functions for cavitating pumps.

2 Pump Transfer Function Data

The linear dynamic transfer matrix for a pump is denoted here by TP_{ij} and is defined by

$$\begin{Bmatrix} P_2 \\ m_2 \end{Bmatrix} = \begin{bmatrix} TP_{11} & TP_{12} \\ TP_{21} & TP_{22} \end{bmatrix} \begin{Bmatrix} P_1 \\ m_1 \end{Bmatrix} \tag{1}$$

where P and m are the complex, linearized fluctuating total pressure and mass flow rate and subscripts 1 and 2 refer to the pump inlet and discharge, respectively (the reader is referred to Ref. [8] for extensive discussion of hydraulic transfer functions and their properties). In general, TP_{ij} will be a function of the frequency, ω, of the perturbations and the mean flow conditions in the pump, including the design, the cavitation number, σ, and the flow coefficient. In this review, we will focus primarily on the second of these equations and on TP_{21} and TP_{22}, since cavitation has a major effect on these characteristics and they therefore have a critical influence on the potential instabilities in the fluid system in which the pump is installed [7]. But it is valuable in passing to note that $TP_{12} = -R - j\omega L$, where R is the pump resistance and L is the pump inertance (valuable measurements of these dynamic characteristics for a noncavitating pump were first made by Ohashi [9] and by Anderson et al. [10]). In the absence of cavitation and compressibility effects, $TP_{11} = 1$, but its departure from unity due to the dependence of the pressure rise on cavitation number at fixed flow rate may also be important, particularly at very low cavitation numbers.

The transfer function and other pump dynamic characteristics presented in this paper are nondimensionalized in the manner of Brennen et al. [2]. Specifically, the frequency, ω, is nondimensionalized as $\omega' = \omega h/U_t$, where h is the peripheral blade tip spacing at the inlet to the pump or inducer ($h = 2\pi R_t/N$, where R_t is the inlet tip radius and N is the number of main blades) and U_t is the inlet tip speed ($U_t = \Omega R_t$, where Ω is the rotational speed in rad/s). Then, the compliance, C, and mass flow gain factor, M, are defined by expanding the transfer function elements, TP_{21} and TP_{22}, at low frequency in power series in $j\omega$,

$$TP_{21} = -j\omega C + (j\omega)^2 C^* + \ldots \tag{2}$$

$$TP_{22} = 1 - j\omega M + (j\omega)^2 M^* + \ldots \tag{3}$$

The compliance, C, and mass flow gain factor, M, are nondimensionalized by

$$\frac{CN\Omega^2}{4\pi^2 R_t} \quad \text{and} \quad \frac{MN\Omega}{2\pi} \tag{4}$$

Note that the above nondimensionalization scheme differs from that used in Brennen [8] but is preferred, since each blade produces cavitation that contributes to C and M.

Those first experimental measurements of the complete dynamic transfer function for a cavitating pump [1,2] were carried out in water with a series of model inducers, including a scale model of the low pressure LOX inducer in the space shuttle main engine (SSME). A typical photograph of the 10.2-cm-diameter version of that inducer under moderate cavitating conditions is included as Fig. 1, which illustrates the tip clearance backflow and cavitation that is typical of many inducers [8].

Measured transfer functions for that 10.2-cm-diameter SSME inducer operating in water at 6000 rpm, a flow coefficient of $\phi_1 = 0.07$, and various cavitation numbers, σ, are reproduced in Fig. 2 (left), where the four transfer functions elements are each plotted against a dimensionless frequency: the real parts as the solid lines and the imaginary parts as dashed lines. We should note that this data necessarily has substantial uncertainty associated with it (primarily because of the difficulty of accurately measuring the unsteady flow rates [1,2]) and therefore polynomial fits in the Laplace variable $j\omega$ were produced in order to extract quantities like R, L, C, and M (the polynomial fits to Fig. 2 (left) are shown in Fig. 2 (right)).

An up-to-date collection of the available data on the compliance and the mass flow gain factor is presented in Fig. 3, where those quantities are plotted against the cavitation number. The data on the 10.2-cm SSME inducer in water was extracted from Fig. 2; the data for the 7.6-cm SSME inducer is more scattered because of greater uncertainty in the measurements of the transfer functions for that smaller model [1]. The old J2 oxidizer data was derived by Brennen and Acosta [11] using test data and a heuristic dynamic model of the test facility. The LE-7 test data in liquid nitrogen was obtained by Shimura [12]. The LE-7A data is the only LOX data and was also extracted from test data by Hori and Brennen [13]. For a full description of the derivation of the J2, LE-7, and LE-7A data extraction, the reader is referred to

Contributed by the Fluids Engineering Division of ASME for publication in the JOURNAL OF FLUIDS ENGINEERING. Manuscript received March 26, 2012; final manuscript received November 30, 2012; published online April 8, 2013. Assoc. Editor: Olivier Coutier-Delgosha.

Fig. 1 Scale model of the low pressure liquid oxygen pump impeller for the space shuttle main engine (SSME) in moderate cavitating conditions in water

Refs. [11–13] and references therein. All of this data is subject to significant uncertainty (due to a combination of uncertainty in the hypothesized dynamic model or in the measurement of the unsteady flow rates), though the original SSME data is probably the most reliable, since it is based on measurements of the complete dynamic transfer function and not on any hypothesized dynamic model. Nevertheless, with one exception, both the compliance and mass flow gain factor data exhibit significant consistency, in which both C and M are inversely proportional to σ. The exception is the LE-7A LOX data for the mass flow gain factor; whether this discrepancy is within the uncertainty band or an actual LOX thermal effect remains to be seen.

Before further discussion of this data collection, we digress briefly to introduce a property in the dynamics of cavitating pumps that has not received sufficient attention in the past, namely, the fundamental resonant frequency of a cavitating pump.

3 Resonant Frequency of a Cavitating Pump

It has been known for a long time that a cavitating inducer or pump may exhibit a violent surge oscillation at subsynchronous frequencies that results in very large pressure and flow rate oscillations in the system of which the pump is a part [10,14–19]. In the early days, this was known as "auto-oscillation," but the preferred name in recent times has been "cavitation surge." It typically occurs at low cavitation numbers just above those at which cavitation head loss becomes severe. Often, it is preceded by a rotating cavitation pattern (see, for example, Refs. [19–22]). Figure 4 reproduces data on the frequencies of oscillation observed for the model SSME inducer and for a helical inducer by Braisted and Brennen [18]; they also plotted a rough empirical fit to that data, which approximated the dimensionless surge frequency by $(5\sigma)^{1/2}$. More recently, we recognize that this "natural frequency of a cavitating pump" has a more fundamental origin as follows: Almost any reasonable, proposed dynamic model for a cavitating inducer or pump (such as that on the right of Fig. 4 designed to simulate the parallel streams of main flow and tip clearance flow) that incorporates both the pump inertance, L, and the cavitation compliance, C, clearly exhibits a natural frequency, Ω_P, given by

$$\Omega_P = \frac{1}{(LC)^{1/2}} \tag{5}$$

Using the data for the SSME LOX inducer from Brennen [8], we can approximate L and C by

$$L \approx \frac{10}{R_t} \quad \text{and} \quad C \approx \frac{0.05\,R_t}{\sigma\Omega^2} \tag{6}$$

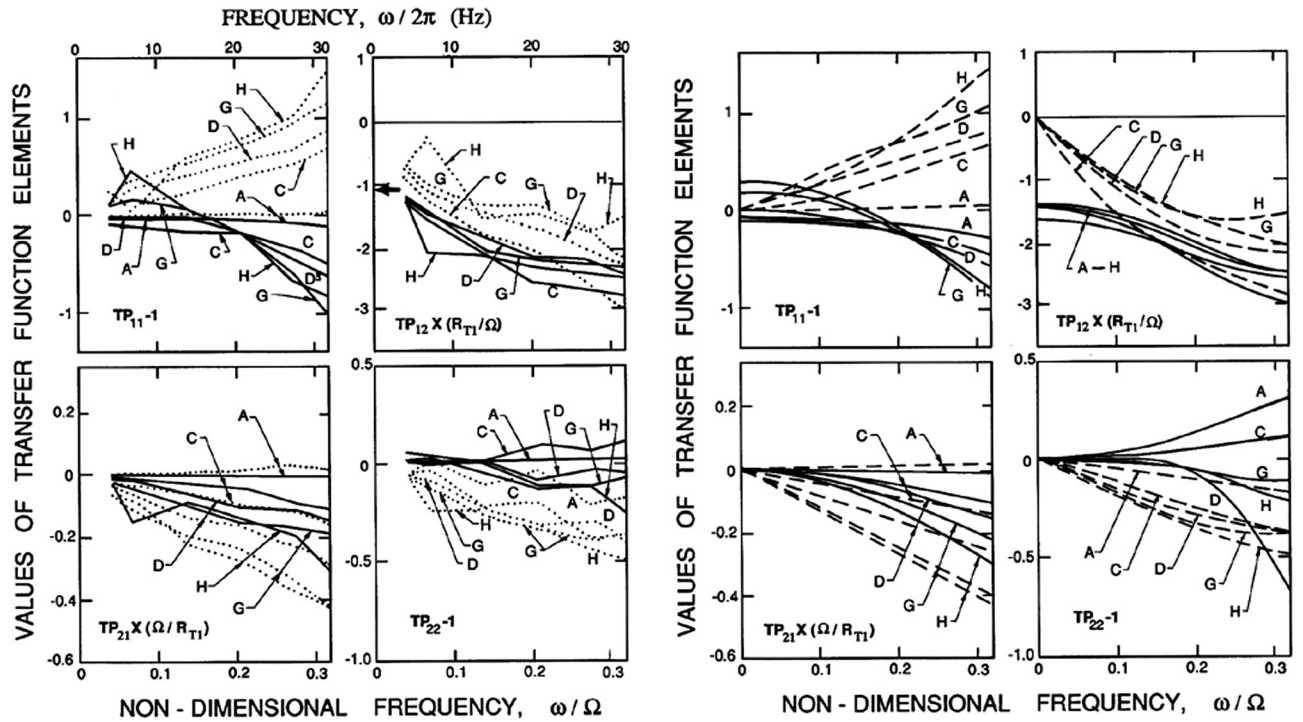

Fig. 2 Left: Typical transfer functions for a cavitating inducer obtained by Brennen et al. [2] for the 10.2-cm-diameter SSME inducer operating in water at 6000 rpm and a flow coefficient of $\phi_1 = 0.07$. Data is shown for four different cavitation numbers, $\sigma =$ (A) 0.37, (C) 0.10, (D) 0.069, (G) 0.052, and (H) 0.044. Real and imaginary parts are denoted by the solid and dashed lines, respectively. The quasistatic pump resistance is indicated by the arrow. Right: Polynomial curves fitted to the data on the left. Adapted from Brennen et al. [2].

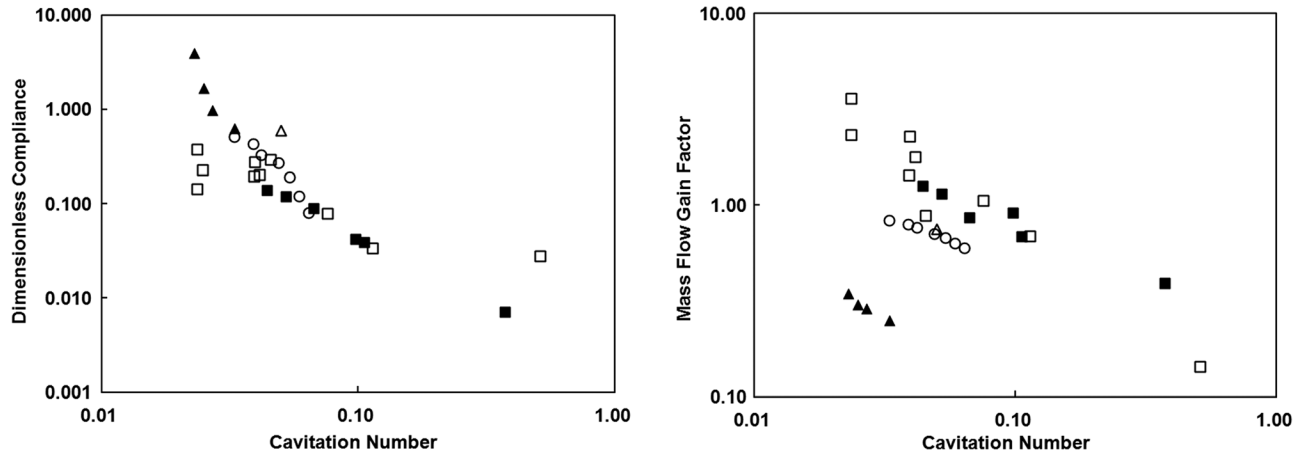

Fig. 3 Dimensionless cavitation compliance (left) and mass flow gain factor (right) plotted against tip cavitation number for: (*a*) Brennen et al. [2] SSME 10.2-cm model inducer in water (solid squares); (*b*) Brennen et al. [2] SSME 7.6-cm model inducer in water (open squares); (*c*) Brennen and Acosta [11] J2-Oxidizer (circles) analysis; (*d*) Hori and Brennen [13] LE-7A LOX data (solid triangles); (*e*) Shimura [12] LE-7 LN2 data (open triangles)

so that, substituting into Eq. (5),

$$\frac{\Omega_P}{\Omega} \approx (2\sigma)^{1/2} \quad \text{or} \quad \Omega'_P \approx \frac{\Omega_P h}{U_t} \approx (5\sigma)^{1/2} \tag{7}$$

This is precisely the same as the result proposed empirically by Braisted and Brennen [18] and shown on the left in Fig. 4. We will refer to this as the natural frequency of a cavitating pump. Indeed the data of Fig. 4 (left) displays further detail of this cavitating pump property. There is a manifest trend for the frequency to decrease somewhat with flow coefficient, and this seems certain to be the result of an increasing volume of cavitation and increasing compliance as the blades are loaded up at lower flow coefficients.

It is important to emphasize that this does not necessarily mean that the major system instability oscillations occur at this frequency. The study of Hori and Brennen [13] discussed later in this paper shows, however, that major instabilities or resonances can occur when this natural frequency for a cavitating pump coincides with other system frequencies, such as an organ pipe mode in a suction or discharge tube.

4 Phase Lags in the Cavitation Dynamics

Several researchers [23–25] have pointed out that the compliance and mass flow gain factor may become complex as the frequency increases and that this can have important consequences for launch vehicles. This is clearly equivalent to significant values of the quadratic terms in the expansions (8) and (9), but Rubin [25] puts the values of C^* and M^* in terms of a compliance phase lag and a mass flow gain factor phase lag. One can visualize these phase lags as delays in the cavitation volume response to the pressure and incidence angle perturbations, respectively. In this paper, we will follow Rubin in writing the expansions (8) and (9) up to and including the quadratic order as

$$TP_{21} = -j\omega C\{1 - j\omega'\tau_C\} \tag{8}$$

$$TP_{22} = 1 - j\omega M\{1 - j\omega'\tau_M\} \tag{9}$$

where τ_C and τ_M are the nondimensional compliance phase lag and mass flow gain factor phase lag, respectively. Data on these quadratic terms in the frequency expansions is, of course, subject to even greater uncertainty than the linear terms that lead to the compliance and mass flow gain factor. Nevertheless, in the light of the increasingly apparent importance of these terms, we have extracted values of τ_C and τ_M from the data of Fig. 2 (right) and plotted them against cavitation number in Fig. 5. Note that the uncertainties in this data probably exceed 50%. Nevertheless, we might suggest that the phase lags appear to be roughly independent of the cavitation number and to be somewhat greater for the compliance than for the mass flow gain factor.

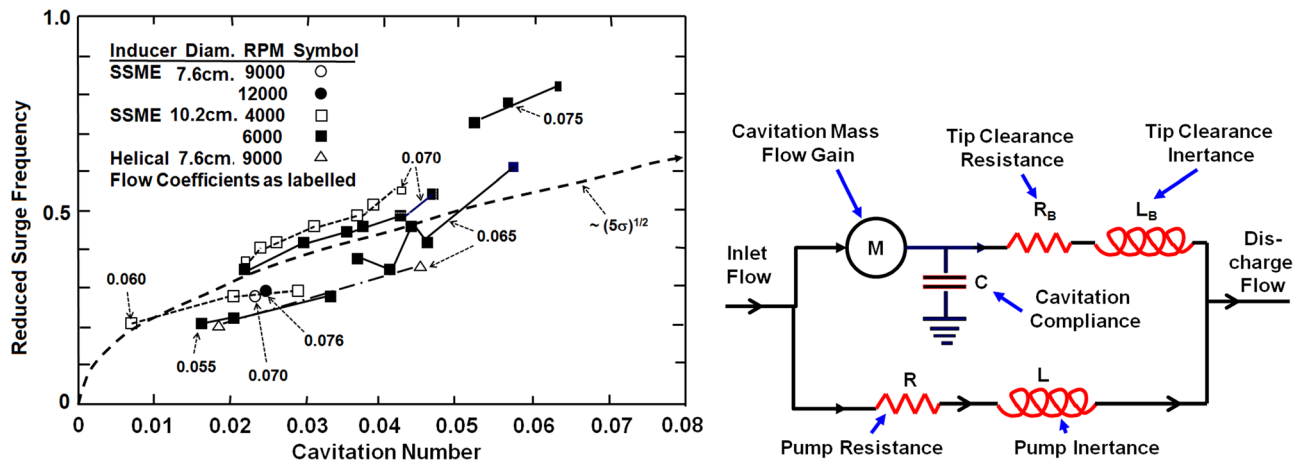

Fig. 4 Left: Nondimensional cavitation surge frequency as a function of cavitation number for the SSME model inducers at various speeds and flow coefficients, as shown. The theoretical prediction is the dashed line, $(5\sigma)^{1/2}$ (adapted from [18]). Right: A dynamic model of the main flow and the parallel tip clearance backflow in a cavitating inducer.

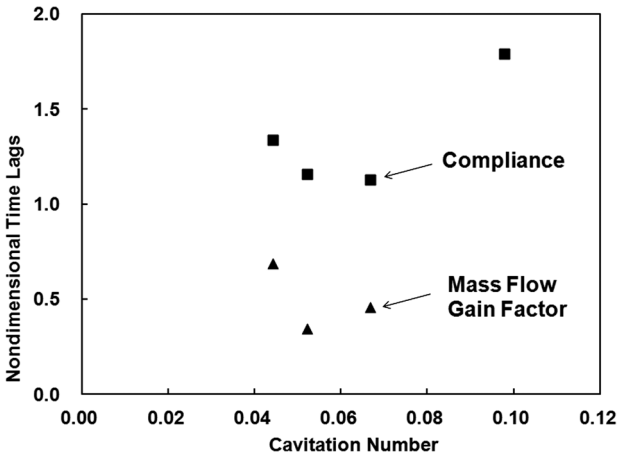

Fig. 5 Nondimensional time lags for the compliance, τ_C, and the mass flow gain factor, τ_M, as functions of the cavitation number for the SSME 10.2-cm model inducer in water. Taken from the data of Brennen et al. [2].

It may be valuable to make some tentative suggestions regarding these phase lags. It seems physically reasonable to envisage that a stream of cavitating bubbles (for example, that carried forward by the backflow) would not respond immediately to the inlet pressure and flow rate fluctuations but would exhibit a phase lag delay that would increase with the frequency of the perturbations. Brennen [23] investigated the compliance of a simple stream of cavitating bubbles at various frequencies, cavitation numbers, and cavitation nuclei sizes. Figure 6 reproduces several figures from that paper, which show that the compliance becomes increasingly complex as the frequency of the perturbations increases and that the negative imaginary parts of the compliance, which develop as the frequency increases, represent just the kind of phase lag that we are addressing here (the magnitudes of the compliance in Fig. 6 are not relevant to the current discussion). It is particularly interesting to observe that the reduced frequency plotted horizontally is defined as fL_s/U_s, where f is the perturbation frequency (in Hz) and L_s and U_s are, respectively, the length and velocity of the simple stream of cavitating bubbles studied. Note from Fig. 6 that the phase lag becomes important when the reduced frequency increases beyond a value of about 0.1. Note also that the frequency, $fL_s/U_s \approx 1$, is a *kinematic* frequency associated with the entry and exit of bubbles from the cavitating zone rather than a *dynamic* frequency associated with the oscillation of the cavitation volume.

Let us consider the corresponding reduced frequency for the backflow cavitation in the experiments of Brennen et al. [2] and Fig. 2. For a 10.2-cm-diameter inducer at a speed of 6000 rpm, a flow coefficient of $\phi_1 = 0.07$ (so that $U_s \approx 200\,\mathrm{cm/s}$), and an estimate length L_s of about 10 cm, the actual frequency that corresponds to $fL_s/U_s = 1$ is $f = 20$ Hz. This corresponds well to the frequency in Fig. 2 at which the imaginary parts of the compliance are observed to become well developed. However, this proposed physical explanation of the compliance phase lag also has some worrying implications. It suggests that the scaling of the phase lags may be a cause for concern, for, at much higher rotational speeds, the phase lag would be much smaller and, consequently, any stability benefit that might accrue from it would be much smaller. However, in the absence of any hard evidence for the scaling of these quadratic effects, all we can conclude at present is that more measurements over a broader range of rotational speeds is needed in order to establish appropriate scaling for the phase lags.

We should note before leaving this topic that Otsuka et al. [24] show that a blade cavitation model can also yield complex compliances and mass flow gain factors that correspond to time lags qualitatively similar to those presented in Fig. 5.

5 Comments on Some Analytical Models

We comment in the conclusions on the difficulties with any detailed computational fluid dynamics (CFD) approach that aims

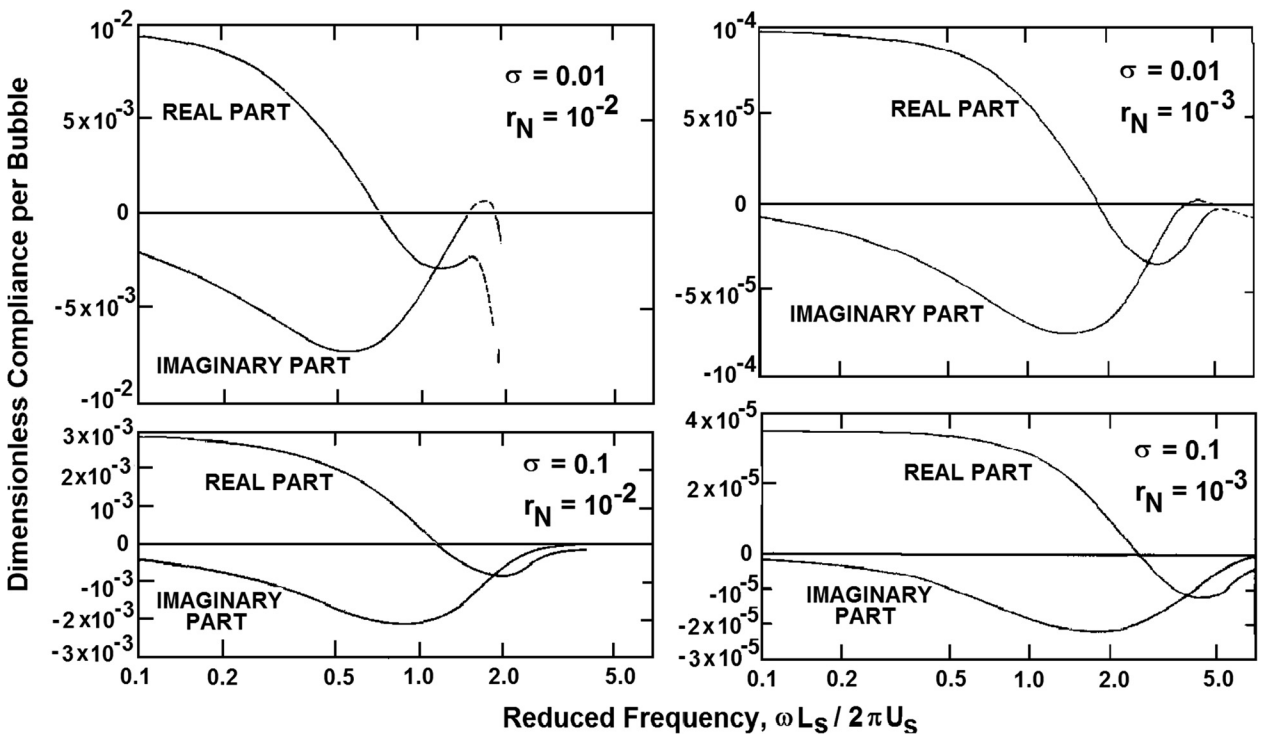

Fig. 6 Real and imaginary parts of the dimensionless compliance (per bubble) of a stream of cavitating bubbles as functions of a reduced frequency based on the length of the cavitation zone, L_s, and its typical velocity, U_s. Results shown for several cavitation numbers, σ, and bubble nuclei size, r_N (from Ref. [23]).

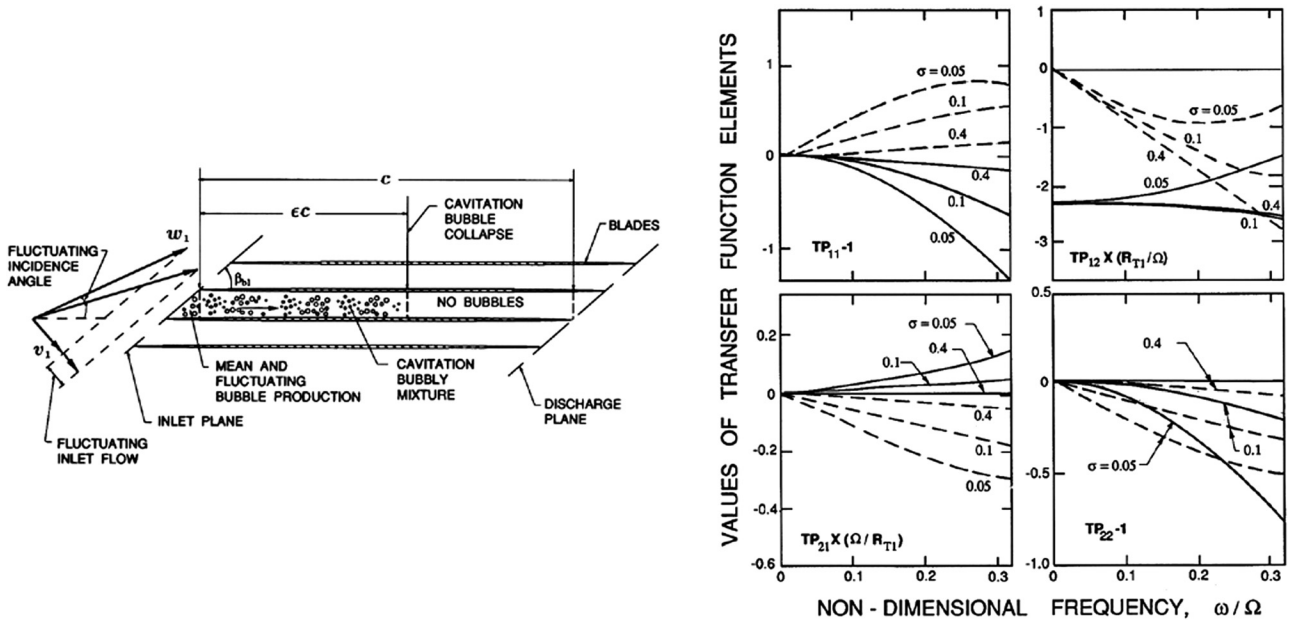

Fig. 7 Left: Schematic of the bubbly flow model for the dynamics of cavitating pumps. Right: Transfer functions for the SSME inducer at $\phi_1 = 0.07$ calculated from the bubbly flow model (adapted from Ref. [27]).

to predict the dynamic transfer function for a cavitating inducer. It seems clear that much progress in developing reduced order models for cavitation in the complex geometry of an inducer (and, in particular, for the backflow cavitation) will be needed before this approach will provide practical and useful guidance. However, in the short-term crude, one-dimensional models and lumped parameter models (see, for example, Cervone et al. [26]) guided by the existing data base can give useful benchmarks. The bubbly flow model of Brennen [27] (see Fig. 7 (left)) incorporated several of the basic phenomena that we now know are inherent in the dynamic response of an inducer or pump, in particular, the compliance of the bubbly stream within the flow (though the compressibility of that bubbly flow had to be represented by an empirical constant, K') and the magnitude of the void fraction fluctuations produced by the fluctuating angle of attack (represented by a second empirical factor of proportionality, M'). These two features respectively lead to dynamic waves and to kinematic waves in the bubbly blade passage flow. A typical transfer function derived from the bubbly flow model is reproduced in Fig. 7 (right), and the similarity with the transfer functions in Fig. 2 (right) is encouraging, even though the two constants K' and M' were empirically chosen.

The measured compliances and mass flow gain factors for the SSME inducers and for the J2 oxidizer inducer are reproduced in Fig. 8 in order to compare that data with several predictions from the bubbly flow model (dashed lines for several choices of K' and M'). The predictions appear to provide a useful benchmark for future data evaluation and comparison.

Figure 8 also includes predictions from the blade cavitation analysis presented earlier by Brennen and Acosta [11]. That analysis has the advantage that it does not contain any empirical parameter as such. However, it assumes that all the cavitation is contained within a single cavity attached to each blade. Moreover, the comparisons in Fig. 8 suggest that such a model does not yield

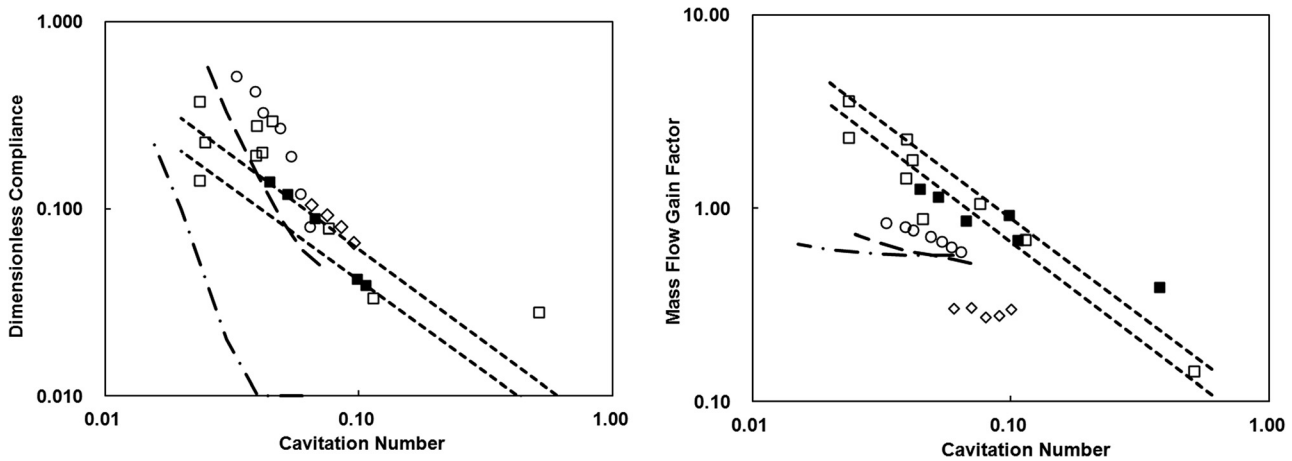

Fig. 8 Dimensionless cavitation compliance (left) and mass flow gain factor (right) plotted against tip cavitation number for: (*a*) Brennen et al. [2] SSME 10.2-cm model inducer in water (solid squares); (*b*) Brennen et al. [2] SSME 7.6-cm model inducer in water (open squares); (*c*) Brennen [27] bubbly flow model results (short dash lines); (*d*) Brennen and Acosta [11] SSME low pressure oxidizer turbopump blade cavitation prediction (dot dash line); (*e*) Brennen and Acosta [11] J2-Oxidizer data (circles); (*f*) Brennen and Acosta [11] J2-Oxidizer blade cavitation prediction (long dash line); (*g*) Yonezawa et al. [28] quasistatic CFD cascade data (diamonds)

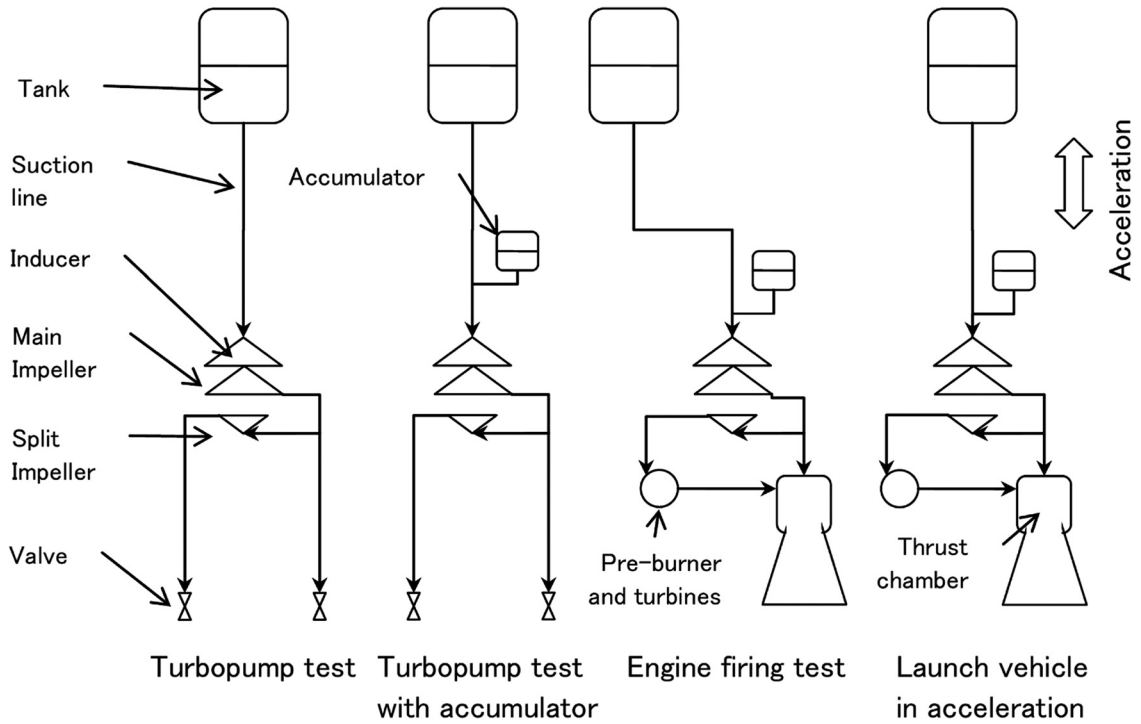

Fig. 9 The four hydraulic system configurations whose dynamic responses are compared (reproduced from Ref. [13])

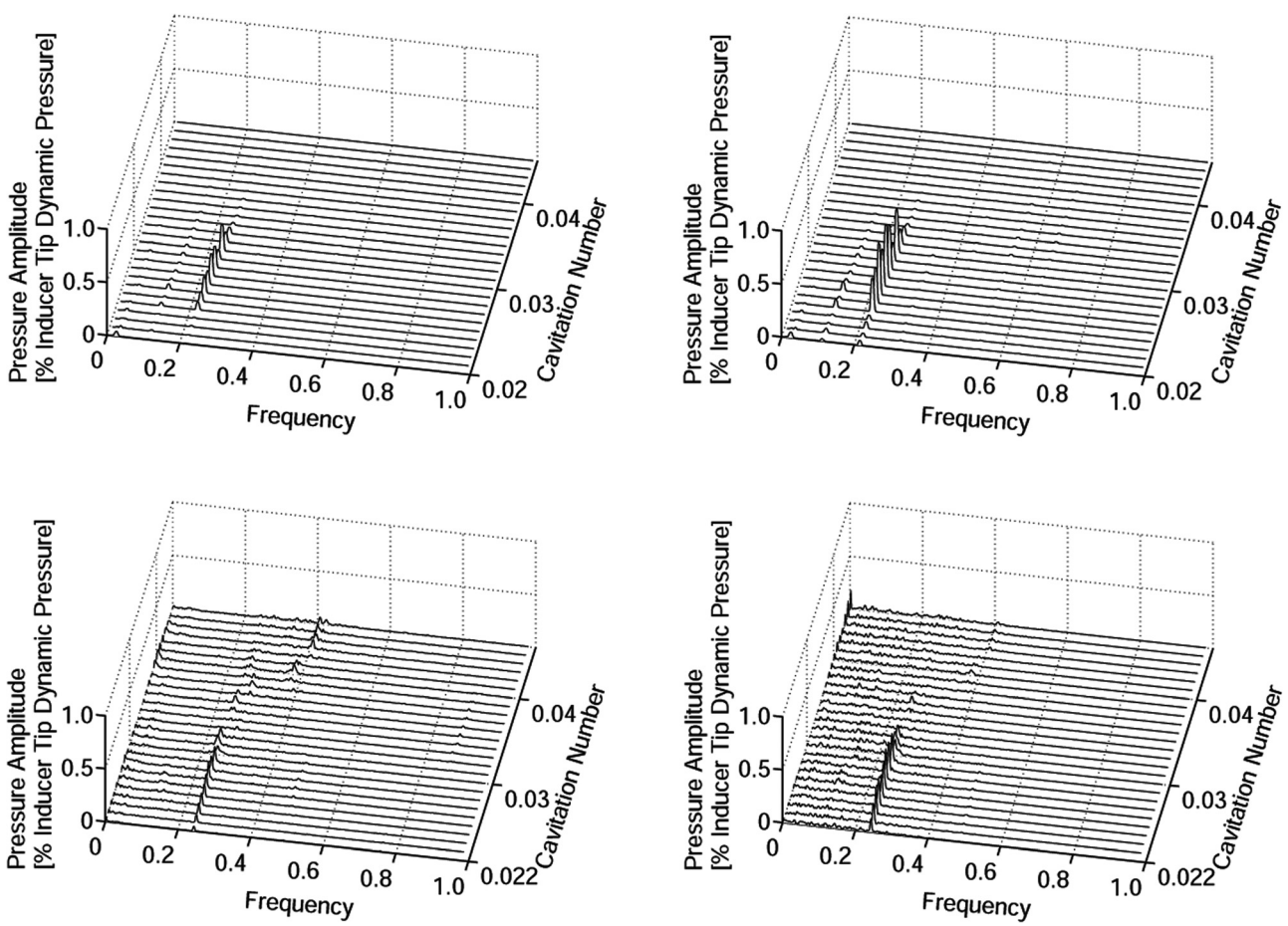

Fig. 10 Model calculations (upper graphs) and test facility measurements (lower graphs) of the pump inlet pressure (left) and the inducer discharge pressure (right) from the cold test facility without an accumulator, the first configuration (reproduced from Ref. [13])

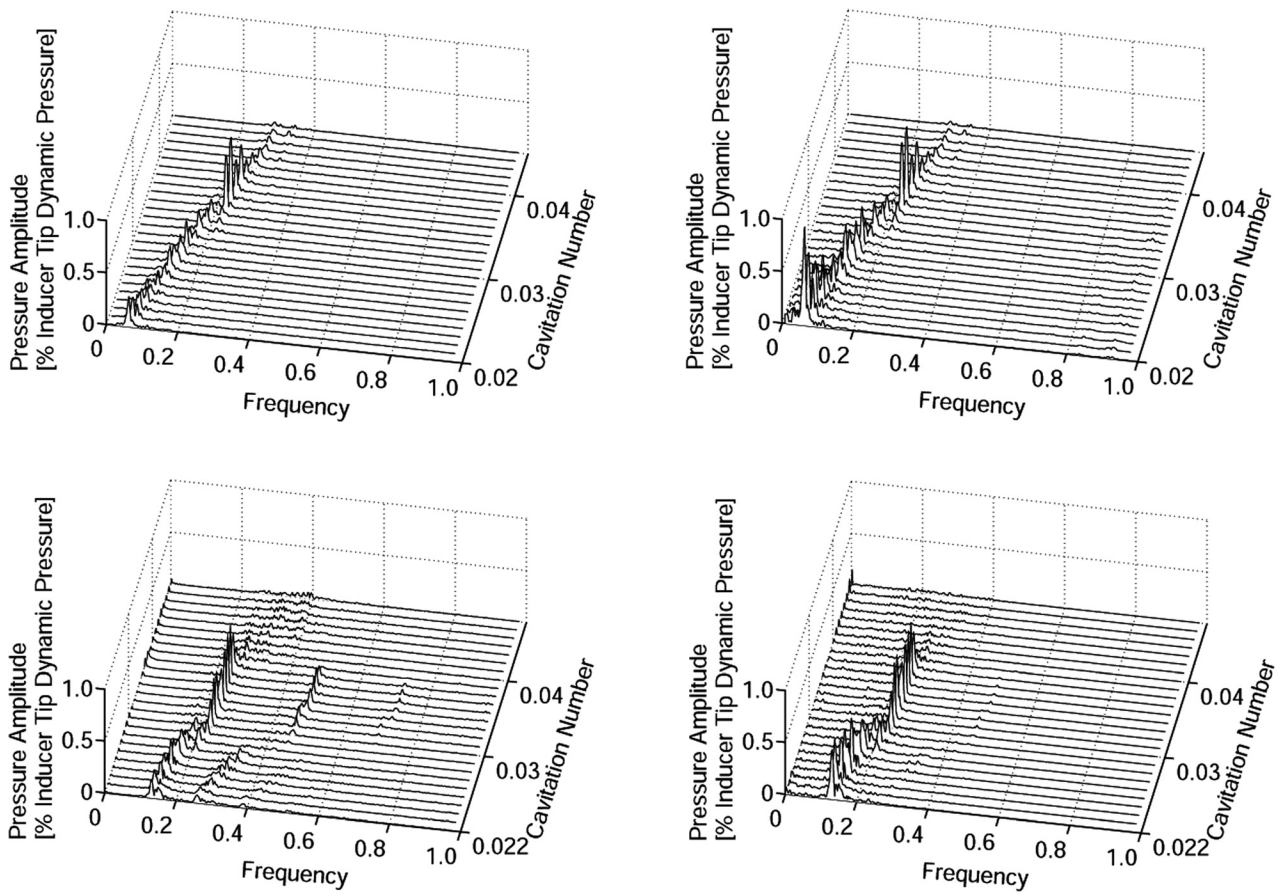

Fig. 11 Model calculations (upper graphs) and test facility measurements (lower graphs) of the pump inlet pressure (left) and the inducer discharge pressure (right) from the cold test facility with an accumulator, the second configuration (reproduced from Ref. [13])

very useful results, which is not surprising when photographs, such as Fig. 1, indicate that the cavitation is primarily bubbly cavitation and not blade cavitation [8].

Also included in Fig. 8 are some quasistatic compliances and mass flow gain factors very recently derived by Yonezawa et al. [28] from steady CFD calculations of the cavitating flow in linear cascades. They have also performed calculations at a series of flow coefficients that show a general trend of increasing compliance and mass flow gain factor as the flow coefficient is decreased.

6 Resonances in Globally Oscillating Systems

The research literature clearly exhibits a strong bias toward investigations of flow instabilities in systems which are essentially at rest, usually in a research laboratory test stand. While this bias is understandable, it can be misleading, for it tends to mask the difference between such flow instability and the resonant response in a flow system subject to global fluctuation. This is particularly an issue with launch vehicle propulsion systems, for they can exhibit some serious resonances with the oscillating vehicle structure. Following the approach originally developed by Rubin [3], Hori and Brennen [13] recently constructed a time-domain model for prototypical pumping systems in order to examine the response of those systems to globally imposed acceleration, $a(t)$. We review those results here, for they present a case in which the static ground-based systems appear free of serious instability, but the same system exhibits serious resonance when subjected to global oscillation.

Hori and Brennen [13] constructed dynamic models for four different configurations used during the testing and deployment of the LOX turbopump for the Japanese LE-7A rocket engine. As sketched in Fig. 9, these configurations include three ground-based facilities, two cold-test facilities (one with a suction line accumulator and the other without), and a hot-fire engine test facility. The fourth configuration is the flight hardware. All four configurations include the same LE-7A turbopump, whose cavitation compliance and mass flow gain factor were extracted from the ground tests and were included in Fig. 3.

The dynamic model for these LE-7A turbopump systems incorporated the time domain equivalent of the pump transfer function, including pump cavitation compliance and mass flow gain factor terms as well as the known steady pump performance characteristic. It also included lumped parameter models for the storage tank (fuel or oxidizer), the accumulator, and the valves, as well as compressible, frictional flow equations for the flows in the feedlines. The assumed boundary conditions at inlet to and discharge from these hydraulic systems were an assumed storage tank pressure and the back pressure in the combustion chamber or catchment tank. Additional pseudopressure terms [29] were included in the flight configuration to account for the globally imposed acceleration, a. These model equations were solved numerically in the time domain using the traditional methods of fluid transients [8,30], including the method of characteristics for the feedlines. Low-level white noise pressure perturbations were injected at the pump inlet in order to provide a trigger for potential cavitation surge, should that be inclined to occur. This technique is based on the assumption that the cavitation surge (and other dynamic responses) observed in the ground-based tests are similarly triggered by random pressure noise.

7 Comparing the System Response and Stability

The results that Hori and Brennen [13] obtained for the four LE-7A test systems are presented in Figs. 10–13. In the case of

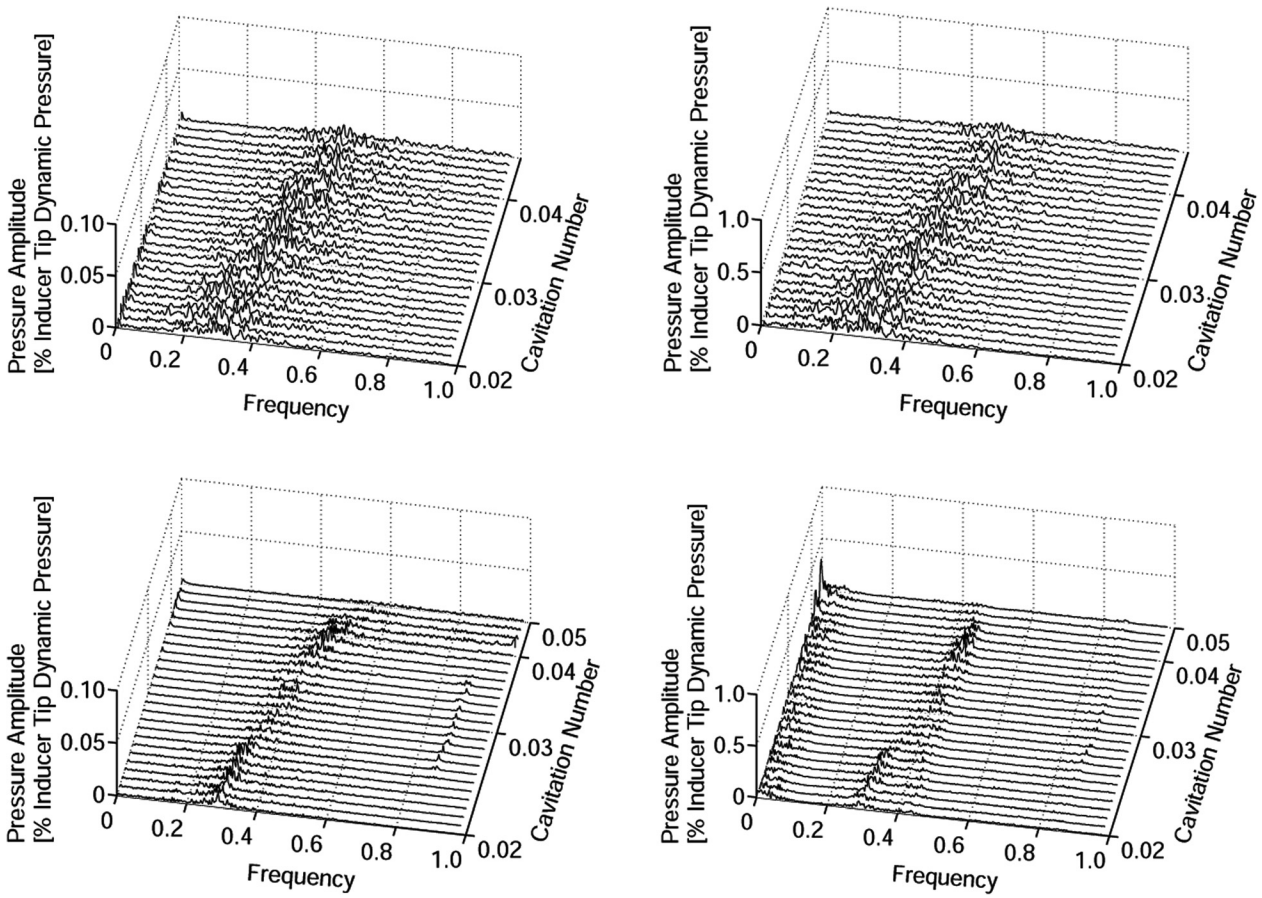

Fig. 12 Model calculations (upper graphs) and test facility measurements (lower graphs) of the pump inlet pressure (left) and the inducer discharge pressure (right) from the hot-firing engine test, the third configuration (reproduced from Ref. [13])

the first three ground-based configurations, comparison is made with pressure spectra obtained during the system testing.

The calculated and measured spectra for the first configuration are shown in Fig. 10 and show excellent agreement. For a cavitation number greater than 0.04, the pressure fluctuations are very small indeed. However, when the cavitation number is decreased into the range 0.033 to 0.020, pressure fluctuations at a nondimensional frequency of 0.22 become dominant; as described earlier, this is the natural frequency of the cavitating pump, and the increase occurs when there is a resonance between that natural frequency (which decreases as σ decreases) and the third organ pipe mode of oscillation of the suction line. However, even these resonant pressure oscillations are inconsequential; for example, the amplitude at the inducer discharge is less than 0.4% of inducer tip dynamic pressure. Note that the spectra also include very small pressure fluctuations at nondimensional frequencies of 0.13 and 0.31; these correspond to the second and the fourth organ pipe modes of the suction line.

Sample results for the second configuration, a different cold-test facility with an accumulator, are presented in Fig. 11. The most obvious change from the first configuration is the appearance of a natural resonant oscillation of the flow between the accumulator and the cavitation in the pump. This occurs because of the short length (and therefore small inertance) of fluid between the accumulator and the cavitation. As the cavitation number decreases and the cavitation compliance increases, the frequency of this natural cavitation surge decreases. For $\sigma > 0.040$, the inducer pressure fluctuations involved are very small. But when σ is reduced to 0.037, a double resonance occurs, involving the natural frequency of the cavitating pump, the frequency of oscillation of the fluid between the accumulator and the pump, and the third organ pipe mode of the feedline between the tank and the pump. This double resonance results in a sudden, substantial increase in the magnitude of the pressure oscillations. With further decrease in σ to 0.035, the fluctuation magnitude decreases again as the double resonance has passed. The corresponding experimental spectra exhibit good qualitative agreement with the model calculations; the higher harmonics observed in the test and which do not appear in the model calculations are probably caused by nonlinear effects. However, despite this double resonance, both the tests and the calculations exhibit very small pressure oscillation amplitudes and less than 1% of inducer tip dynamic pressure, and as in the first configuration, this magnitude is inconsequential.

Spectra for the third configuration, the hot-firing engine test, are shown in Fig. 12. As in the second configuration, the response is dominated by a strong resonance of the fluid between the pump and the accumulator. The frequency of this resonance decreases from 0.5 to 0.2 as the cavitation number is decreased from 0.05 to 0.02 (the frequencies are higher than in the second configuration because the accumulator is much closer to the turbopump). Again, the model results appear to simulate the test data very well, matching both the frequency and the amplitude. However, the pressure amplitudes are still very small, less than 0.01% of the inducer tip dynamic pressure. Even when the peak frequency matches one of the suction line organ pipe frequencies, no large pressure oscillation magnitudes occur, because the suction line in the hot-firing engine test facility is very long and the suction line resistance is large.

Having, to some extent, validated the model calculations, Hori and Brennen [13] then turned to the flight configuration. First, the response of the flight configuration without imposed acceleration was investigated and only very small pressure oscillations (less than 0.01% of inducer tip dynamic pressure) and flow rate oscillations (less than 0.01% of mean flow) were calculated. Thus, like

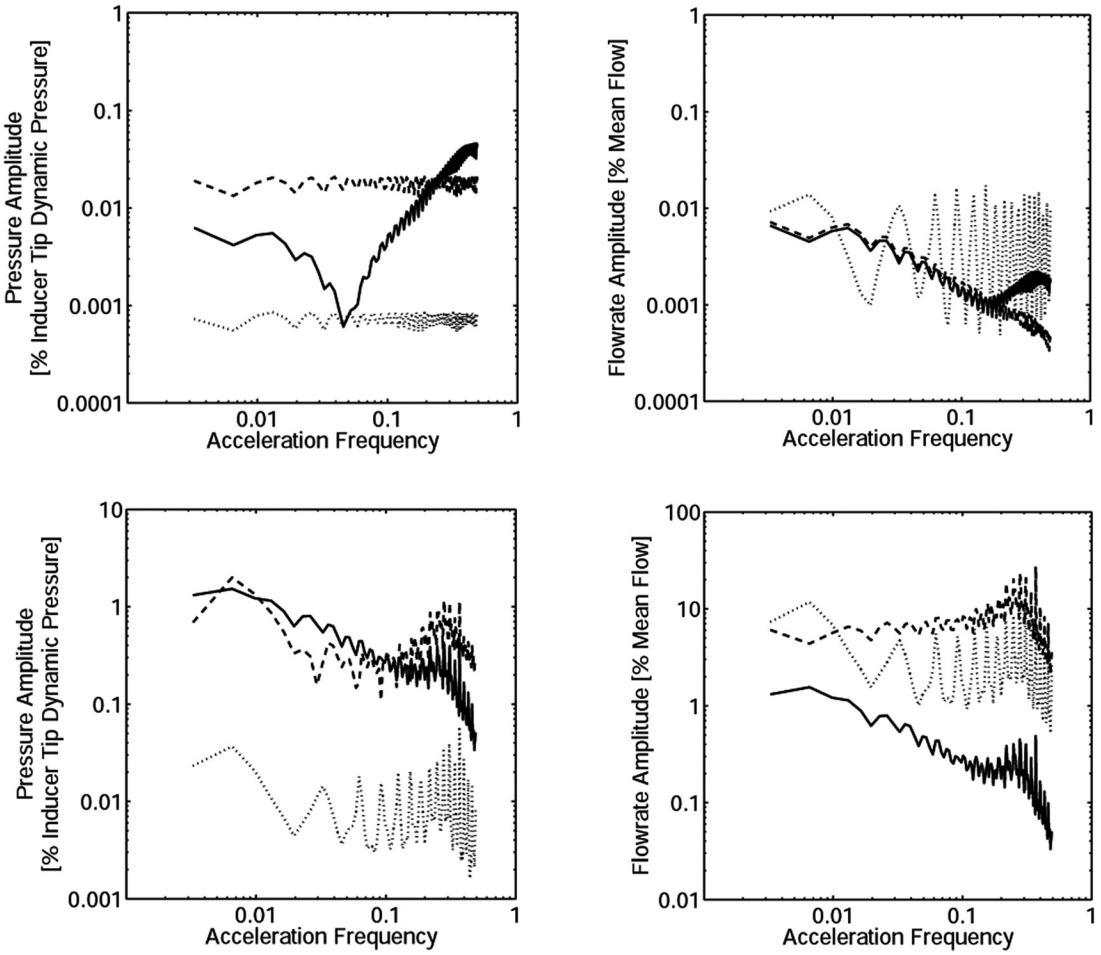

Fig. 13 Model calculations for the flight configuration subject to global acceleration. Upper graphs: in the absence of pump cavitation. Lower graphs: when the pump cavitation number is $\sigma = 0.02$. Pressure amplitudes (left) and flow rate amplitudes (right) over a wide range of different oscillation frequencies and an oscillating acceleration magnitude of $0.1\,\mathrm{m/s^2}$. Solid, dashed, and dotted lines, respectively, present the pump discharge, inducer inlet, and tank outlet quantities (reproduced from Ref. [13]).

the first three configurations, the flight configuration is very stable in a nonaccelerating frame. Then, the model was used to examine the response of the flight configuration in a sinusoidally accelerating frame with an acceleration amplitude of $0.1\,\mathrm{m/s^2}$ at various nondimensional frequencies ranging from 0 to 0.5. The magnitude $0.1\,\mathrm{m/s^2}$ would be characteristic of the background excitation experienced in the rocket environment. Typical model results under noncavitating conditions are shown in the upper graphs of Fig. 13 and are similar in magnitude to the results for the ground-based calculations; the conclusion is that, in the absence of cavitation, the system response is quite muted with pressure oscillation magnitudes less than 0.05% of inducer tip dynamic pressure and flow rate oscillation magnitudes less than 0.02% of mean flow.

Finally, Hori and Brennen [13] present their key result, namely, the response of the flight configuration to the same range of global oscillation (an acceleration magnitude of $0.1\,\mathrm{m/s^2}$ for a range of oscillation frequencies) when the pump is cavitating. The lower graphs of Fig. 13 present the results for the lowest cavitation number examined, namely, $\sigma = 0.02$. It is clear that the result is a violent resonant response with amplitudes about two orders of magnitude greater than in the absence of cavitation. The pressure oscillation magnitudes are more than 2% of inducer tip dynamic pressure, and the flow rate oscillation magnitudes are more than 20% of mean flow. Under these cavitating conditions, the largest flow rate magnitudes occur between the accumulator and the inducer at all frequencies, and the largest pressure amplitudes occur at the inducer discharge. Thus, the flow rate oscillation between the accumulator and the inducer dominates the overall response and excites the rest of the system like an oscillating piston. The suction line from the tank to the accumulator also plays a role, albeit a secondary role. When the frequency of the "piston" coincides with an organ pipe mode of the compressible liquid between the tank and the cavitating inducer, the entire system exhibits a peak response, and this happens at each of those organ pipe modes. There is also an important global response maximum near the natural frequency of the cavitating pump (0.3); at higher frequencies, the response dies off rather rapidly.

Thus, the model calculations demonstrate how a violent resonant response can occur in the accelerating flight environment when pump cavitation is present and that this response can occur even when all the ground tests (and the model flight calculations without cavitation) indicate a stable and well-behaved response. The difficulty of duplicating these adverse flight environments in any ground test—and therefore of examining such an adverse condition—makes accurate model calculations an almost essential design tool.

8 Concluding Remarks

In concluding this review, we should remark that, despite significant progress in understanding the dynamics of cavitation in pumps and inducers, there is much that remains to be accomplished before an adequate pump system design procedure is

completed. It is, perhaps, most useful in these concluding remarks to identify some of the most glaring gaps in our knowledge.

In terms of accomplishments, we do have a reasonable data base supporting our preliminary understanding of the scaling of the dynamic transfer function with pump size, pump rotating speed (admittedly within a fairly narrow speed range), and cavitation number. The effect of flow coefficient is less well-established, due to the limited range of flow coefficients for which transfer functions have been measured. However, most of that data is in water at roughly normal temperatures. Therefore, the first major deficiency is the lack of experimental data for the thermal effects on the dynamics. Thermal effects on cavitation and on the steady state performance of pumps have been extensively studied and are well known; for example, in the context of cryogenic pumps (see, for example, Brennen [8]), thermal effects in liquid oxygen are important and they are pervasive in liquid hydrogen pumps. But apart from some preliminary tests [2,31,32] and some very limited theoretical considerations [23], little is really known about the thermal effects on the dynamic characteristics of cavitating pumps. Testing in fluids other than water is very limited, though the recent work of Yoshida et al. [32] in liquid nitrogen suggests little thermal effect on cavitation surge. The lack of data is, in large measure, due to the absence of dynamic flow meters for nonaqueous environments. Electromagnetic flow meters have proved invaluable in the water tests, in part, because of their unique ability to measure the cross-sectionally integrated flow rate, irrespective of axisymmetric velocity profile and, in part, because of their dynamic capability. (Electromagnetic meters for cryogenic fluids are not out of the question and should be constructively investigated). It seems likely that thermal effects could substantially dampen the dynamic characteristics, and if so, it would be valuable to confirm or refute this.

Another gap that has become evident in recent years and that has a significant impact on pump system stability is the effect of complex values for the compliance and mass flow gain factor. Though we have described above some very crude data on the phase lags for compliance and mass flow gain factor, this data has very large uncertainties associated with it, and we have little knowledge about how the values scale with speed or size. These effects and their uncertainty strongly suggest that a more extensive transfer function data base is needed that would not only examine the thermal effects but also extend the data to higher speeds. Such experimental investigations should also investigate the nonlinear effects that obviously limit the amplitude of the cavitation instabilities and the resonant responses.

Another major gap in our current understanding has been evident for some time through the work of Rubin [3,4] and others on the response of pump systems in globally oscillating environments and was particularly evident in the work of Hori and Brennen [13] described above. There are some very real questions about the dynamic response of cavitation and of cavitating pumps subjected to translational or rotational acceleration. The only surefire way to answer these questions is to conduct experiments with a pump loop experiment mounted on a shaker table that can impose substantial global oscillations up to frequencies of the order of 50 Hz or more. Given the availability of huge shaker tables for earthquake engineering research and the known destructive consequences of instabilities, such as the Pogo instability of liquid-propelled rockets, it is surprising that such experiments have not been carried out in the past.

Finally, I can anticipate that some will promote the use of computational models for cavitating flows in order to try to bridge these gaps. Though there have been some valuable efforts to develop CFD methods for cascades (see, for example, Iga et al. [33]), the problem with this suggestion is that accurate numerical treatments for cavitating pumps that will adequately represent both the nonequilibrium character of cavitation and adequately respond to flow fluctuations are still in a very early stage of development. Codes that can also handle the complex geometry and turbulence of the flow in an inducer, including the tip clearance backflow, are many years away. It seems clear that much progress will be needed in the development of reduced-order models for cavitation before the computational approach can produce useful, practical results.

Acknowledgment

The author wishes to acknowledge the extensive and valuable support provided by the NASA George Marshall Space Flight Center, Huntsville, AL, during much of the research discussed in this paper. I also owe a great debt to my colleague and collaborator Allan Acosta as well as to numerous students at Caltech, particularly S. L. Huang and David Braisted. The numerous constructive discussions with long-time associates Loren Gross, Henry Stinson, Sheldon Rubin, Jim Fenwick, Tom Zoladz, Kenjiro Kamijo, Yoshi Tsujimoto, and Shusuke Hori are gratefully acknowledged. I also appreciate the support of JAXA, the Japan Aerospace Exploration Agency, in sponsoring the visit of Shusuke Hori to Caltech.

Nomenclature

a = global acceleration of the pumping system
C = cavitation compliance
C^*, M^* = quadratic compliance and mass flow gain factor coefficients
f = frequency in Hz
h = inducer blade tip spacing, $2\pi R_t/N$
j = $(-1)^{1/2}$
K', M' = bubbly flow model parameters
L = pump inertance
L_s = length of the cavitation zone
m = complex fluctuating mass flow rate
M = mass flow gain factor
N = number of main inducer blades
P = complex fluctuating total pressure
R = pump resistance
R_t = radius of the inducer tip
TP_{ij} = pump transfer function elements
U_s = velocity in the cavitation zone
U_t = velocity of the inducer tip
ϕ_1 = inlet flow coefficient
σ = cavitation number
ρ = liquid density
τ_C, τ_M = phase lags of the compliance and mass flow gain factor
ω' = dimensionless frequency, $\omega h/U_t$
ω = dimensional radian frequency
Ω = frequency of rotation of the pump
Ω_P = natural cavitation frequency of the inducer
Ω'_P = dimensionless natural cavitation frequency of the inducer, $\Omega_P h/U_t$

Subscripts

1 = inlet to a component
2 = discharge from a component
B = pertaining to the tip clearance flow

References

[1] Ng, S. L., and Brennen, C. E., 1978, "Experiments on the Dynamic Behavior of Cavitating Pumps," ASME J. Fluids Eng., **100**(2), pp. 166–176.
[2] Brennen, C. E., Meissner, C., Lo, E. Y., and Hoffman, G. S., 1982, "Scale Effects in the Dynamic Transfer Functions for Cavitating Inducers," ASME J. Fluids Eng., **104**(4), pp. 428–433.
[3] Rubin, S., 1966, "Longitudinal Instability of Liquid Rockets Due to Propulsion Feedback (POGO)," J. Spacecr. Rockets, **3**(8), pp. 1188–1195.
[4] Rubin, S., 1970, "Prevention of Coupled Structure-Propulsion Instability (POGO)," NASA Space Vehicle Design Criteria (Structures), Report No. NASA SP-8055.
[5] Oppenheim, B. W., and Rubin, S., 1993, "Advanced Pogo Stability Analysis for Liquid Rockets," J. Spacecr. Rockets, **30**(3), pp. 360–373.

[6] Tsujimoto, Y., Kamijo, K., and Brennen, C., 2001, "Unified Treatment of Instabilities of Turbomachines," J. Propul. Power, **17**(3), pp. 636–643.
[7] Dotson, K. W., Rubin, S., and Sako, B. H., 2005, "Mission-Specific Pogo Stability Analysis With Correlated Pump Parameters," J. Propul. Power, **21**(4), pp. 619–626.
[8] Brennen, C. E., 1994, *Hydrodynamics of Pumps*, Oxford Univ. Press., New York.
[9] Ohashi, H., 1968, "Analytical and Experimental Study of Dynamic Characteristics of Turbopumps," Report No. NASA TN D-4298.
[10] Anderson, D. A., Blade, R. J., and Stevens, W., 1971, "Response of a Radial-Bladed Centrifugal Pump to Sinusoidal Disturbances for Non-Cavitating Flow," Report No. NASA TN D-6556.
[11] Brennen, C. E., and Acosta, A. J., 1976, "The Dynamic Transfer Function for a Cavitating Inducer," ASME J. Fluids Eng., **98**(2), pp. 182–191.
[12] Shimura, T., 1995, "Geometry-Effects in the Dynamic Response of Cavitating LE-7 Liquid-Oxygen Pump," J. Propul. Power, **11**(2), pp. 330–336.
[13] Hori, S., and Brennen, C. E., 2011, "Dynamic Response to Global Oscillation of Propulsion Systems With Cavitating Pumps," J. Spacecr. Rockets, **48**(4), pp. 599–608.
[14] Sack, L. E., and Nottage, H. B., 1965, "System Oscillations Associated With Cavitating Inducers," ASME J. Basic Eng., **87**(4), pp. 917–924.
[15] Rosenmann, W., 1965, "Experimental Investigations of Hydrodynamically Induced Shaft Forces With a Three-Bladed Inducer," Proc. ASME Symp. on Cavitation in Fluid Machinery, pp. 172–195.
[16] Natanzon, M. S., Bl'tsev, N. E., Bazhanov, V. V., and Leydervarger, M. R., 1974, "Experimental Investigation of Cavitation-Induced Oscillations of Helical Inducers," Fluid Mech.-Sov. Res., **3**(1), pp. 38–45.
[17] Miller, C. D., and Gross, L. A., 1967, "A Performance Investigation of an Eight-Inch Hubless Pump Inducer in Water and Liquid Nitrogen," Report No. NASA TN D-3807.
[18] Braisted, D. M., and Brennen, C. E., 1980, "Auto-Oscillation of Cavitating Inducers," *Polyphase Flow and Transport Technology*, R. A. Bajura, ed., ASME, New York, pp. 157–166.
[19] Zoladz, T., 2000, "Observations on Rotating Cavitation and Cavitation Surge From the Development of the Fastrac Engine Turbopump," Proc. 36th AIAA/ASME/SAE/ASEE Joint Propulsion Conf., Huntsville, AL, Paper No. AIAA-2000-3403.
[20] Kamijo, K., Shimura, T., and Tsujimoto, Y., 1994, "Experimental and Analytical Study of Rotating Cavitation," ASME Cavitation and Gas-Liquid Flow in Fluid Machinery and Devices, Lake Tahoe, CA, ASME FED, Vol. 190, pp. 33–43.
[21] Tsujimoto, Y., Kamijo, K., and Yoshida, Y., 1993, "A Theoretical Analysis of Rotating Cavitation in Inducers," ASME J. Fluids Eng., **115**(1), pp. 135-141.
[22] Hashimoto, T., Yoshida, M., Watanabe, M., Kamijo, K., and Tsujimoto, Y., 1997, "Experimental Study on Rotating Cavitation of Rocket Propellant Pump Inducers," J. Propul. Power, **13**(4), pp. 488–494.
[23] Brennen, C. E., 1973, "The Dynamic Behavior and Compliance of a Stream of Cavitating Bubbles," ASME J. Fluids Eng., **95**(4), pp. 533–541.
[24] Otsuka, S., Tsujimoto, Y., Kamijo, K., and Furuya, O., 1996, "Frequency Dependence of Mass Flow Gain Factor and Compliance of Cavitating Inducers," ASME J. Fluids Eng., **118**(2), pp. 400–408.
[25] Rubin, S., 2004, "An Interpretation of Transfer Function Data for a Cavitating Pump," Proc. 40th AIAA/ASME/SAE/ASEE Joint Propulsion Conference, Florida, Paper No. AIAA-2004-4025.
[26] Cervone, A., Tsujimoto, Y., and Kawata, Y., 2009, "Evaluation of the Dynamic Transfer Matrix of Cavitating Inducers by Means of a Simplified 'Lumped-Parameter' Model," ASME J. Fluids Eng., **131**(4), p. 041103.
[27] Brennen, C. E., 1978, "Bubbly Flow Model for the Dynamic Characteristics of Cavitating Pumps," J. Fluid Mech., **89**, pp. 223–240.
[28] Yonezawa, K., Aono, J., Kang, D., Horiguchi, H., Kawata, Y., and Tsujimoto, Y., "Numerical Evaluation of Transfer Matrix of an Inducer Under Cavitating Condition," (unsubmitted manuscript).
[29] Batchelor, G. K., 1967, *An Introduction to Fluid Dynamics*, Cambridge University, Cambridge, England.
[30] Wylie, E. B., Streeter, V. L., and Suo, L., 1993, *Fluid Transients in Systems*, Prentice-Hall, Englewood Cliffs, NJ.
[31] Yoshida, Y., Sasao, Y., Watanabe, M., Hashimoto, T., Iga, Y., and Ikohagi, T., 2009, "Thermodynamic Effect on Rotating Cavitation in an Inducer," ASME J. Fluids Eng., **131**(9), p. 091302.
[32] Yoshida, Y., Nanri, H., Kikuta, K., Kazami, Y., Iga, Y., and Ikohagi, T., 2011, "Thermodynamic Effect on Subsynchronous Rotating Cavitation and Surge Mode Oscillation in a Space Inducer," ASME J. Fluids Eng., **133**(6), p. 061301.
[33] Iga, Y., Nohmi, M., Goto, A., and Ikohagi, T., 2004, "Numerical Analysis of Cavitation Instabilities Arising in the Three-Blade Cascade," ASME J. Fluids Eng., **126**(3), pp. 419–429.